Available online at www.sciencedirect.com
SCIENCE DIRECT®
Journal of Sound and Vibration 285 (2005) 187–207
JOURNAL OF SOUND AND VIBRATION
www.elsevier.com/locate/jsvi

Modified input shaping for a rotating single-link flexible manipulator

Jinjun Shan[a,*], Hong-Tao Liu[a], Dong Sun[b]

[a]*The Institute for Aerospace Studies, University of Toronto, 4925 Dufferin Street, Toronto, Ont., Canada M3H 5T6*
[b]*Department of Manufacturing Engineering & Engineering Management, City University of Hong Kong, 83 Tat Chee Avenue, Kowloon, Hong Kong*

Received 5 March 2004; received in revised form 9 August 2004; accepted 19 August 2004
Available online 22 December 2004

Abstract

Input shaping is a feedforward approach and can be applied to suppress flexible vibration. In this paper, modified input shaping (MIS) is proposed for robustness and multimode vibration suppression. The theoretic analysis shows that the MIS poses better performance in several aspects than the traditional input-shaping technique. The controller that combines MIS with PD feedback law is designed for an experimental single-link flexible manipulator. Hardware experiments are conducted to verify the proposed method.

1. Introduction

Increasing demands for high-speed performance and low energy consumption of robotic systems coupled with needs of space application have motivated the design of light-weight manipulators. Controls of such systems pose challenging problems when the significant flexibility must be taken into account [1,2]. Considerable work has been carried out in the control of flexible manipulators over the past years, which can be roughly divided into feedback and feedforward strategies. The feedback control strategies use measurements and estimations of the system states to suppress vibrations, such as adaptive control [3], fuzzy control [4], sliding mode variable

*Corresponding author. Tel.: +1 416 667 7855; fax: +1 416 667 7799.
E-mail address: shan@utias.utoronto.ca (J. Shan).

0022-460X/$ - see front matter © 2004 Elsevier Ltd. All rights reserved.
doi:10.1016/j.jsv.2004.08.035

structure control [5], neural network control [6], etc. Smart materials have also been used as sensors and actuators in the vibration control, i.e. piezoelectric materials [7], shape memory alloys [8], etc. While feedback approaches have been demonstrated to be effective, the performance of feedback methods can often be improved by adding a feedforward controller.

One special feedforward control strategy, known as input shaping, has been studied widely since its first appearance [9] for possessing the advantages of simplicity and effectiveness, and because no additional sensor and actuator are required. Fig. 1 shows the process of input shaping. With this method, an input command is convolved with a sequence of impulses, called an input shaper, to produce a shaped command that causes less vibration than the original unshaped command. It has been successfully used to reduce residual vibrations in numerous mechanical systems, such as coordinate measuring machines [10,11], experiments on board of the space shuttle Endeavor [12,13], long-reach manipulators [14], cranes [15,16], and two-link flexible manipulators [17].

Many control schemes were successfully implemented by employing the input-shaping technique. Hillsley and Yurkovich [18] apply input shaping to large angle movements of a two-link robot, switched to feedback control when approaching the desired position. A combined controller of input shaper and state feedback is successfully implemented on a five-bar linkage manipulator [19]. Magee and Book [20] incorporate input shaping into a feedback controller to suppress the vibration of a small-articulated robot mounted on the end of a long and slender beam. Ooten and Singhose [21] combine input shaping and sliding mode control to improve the tracking performance of a flexible system. It has been demonstrated by Murphy and Watanabe [22] that the design of input shapers in the z-domain is easy and effective, and that the proposed shaping algorithm could easily adapt the shaper parameters to dynamic systems with parameters variation. Other researches include an extension of the pole-zero cancellation design techniques [23], a particular straightforward approach [24], and the use of the z-plane to design a robust multi-hump input shaper [25]. The design of multi-input shapers using s-plane pole placement technique can be found in Ref. [26]. The maneuver command with input-shaping technique has been designed for flexible spacecrafts with on–off actuators [27,28]. Input shaping is also compared with several traditional filters in Ref. [29]. Input shaping for multimode vibration suppression can be found in Refs. [30,31].

In this paper, the traditional input shaping (TIS) is modified and the modified technique is studied in detail. The remainder of this paper is organized as follows. In Section 2, the TIS is introduced first and then the modified input shaping (MIS) is proposed and analyzed. The model for a kind of single-link flexible manipulator is proposed in Section 3. In Section 4, an experimental single-link flexible manipulator is developed and the experimental results are discussed. Finally, some conclusions are given in Section 5.

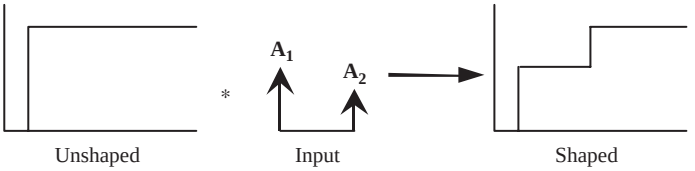

Fig. 1. Diagram of input-shaping process.

2. MIS

To simplify the analysis, a harmonic vibration system is given in Eq. (1):

$$\ddot{x} + 2\varsigma\omega\dot{x} + \omega^2 x = \omega^2 F(t), \tag{1}$$

where x is the state, ω is the natural frequency, ς is the damping ratio, and $F(t)$ is the control input. The corresponding damped vibration frequency ω_d and period T_d can be calculated by $\omega_d = \omega\sqrt{1-\varsigma^2}$ and $T_d = 2\pi/\omega_d$, respectively.

In the following, we use the time domain approach to determine the parameters of the input shaper. The vibration amplitude of system (1) can be derived from the sum of the impulse responses. The response of the vibration system under multiple impulses can be calculated as

$$V(\omega,\varsigma) = \mathrm{e}^{-\varsigma\omega T_m}\left(\left(\sum_{i=1}^{m} A_i \mathrm{e}^{\varsigma\omega T_i}\cos(\omega_d T_i)\right)^2 + \left(\sum_{i=1}^{m} A_i \mathrm{e}^{\varsigma\omega T_i}\sin(\omega_d T_i)\right)^2\right)^{1/2}, \tag{2}$$

where m is the number of applied impulses, A_i and T_i are the amplitude and acting time of the ith impulse. The simplest constraint to put on the system is zero vibration (ZV) at the modeled frequency, and damping of the vibration mode, i.e. $V(\omega_m,\varsigma_m) = 0$, which requires

$$\sum_{i=1}^{m} A_i \mathrm{e}^{\varsigma\omega T_i}\cos(\omega_d T_i) = 0, \quad \sum_{i=1}^{m} A_i \mathrm{e}^{\varsigma\omega T_i}\sin(\omega_d T_i) = 0. \tag{3a,b}$$

To guarantee the desired performance, two more constraints were also imposed: (1) $T_1 = 0$; (2) $\sum A_i = 1$. The first constraint is just for simplification. The second constraint ensures the final set point of the system due to the shaped input is the same as that due to the unshaped input.

There are overall four constraint equations and therefore four unknown variables can be solved. We define the amplitude and the acting time of 2 impulses as four variables. For limiting the actuator saturation, an extra constraint $A_i > 0$ is imposed so that the shaped input will not lead to actuator saturation if the unshaped input does not lead to saturation.

Solving the above equations with constraints, there will be an infinite number of solutions because of the $\sin(\cdot)$ and $\cos(\cdot)$ terms. By minimizing the shaper duration, we can obtain the following closed-form solution for 2 impulses:

$$A_1 = \frac{1}{1+K}, \quad T_1 = 0, \quad A_2 = \frac{K}{1+K}, \quad T_2 = \frac{T_d}{2}, \tag{4}$$

where $K = \mathrm{e}^{-(\varsigma\pi/\sqrt{1-\varsigma^2})}$. The duration of this shaper is T_2.

Eq. (4) was first given in Ref. [32], which is regarded as the original publication on the input-shaping concept. In the TIS technique [9], this 2-impulse shaper is called a ZV shaper because it constrains the vibration amplitude in Eq. (2) to zero at the modeled frequency and damping.

In fact, there are many shapers that can realize ZV at the modeled frequency and damping. For n impulses, if the amplitudes and the acting times satisfy the following, this n-impulse shaper can

also achieve ZV [33]:

$$\begin{aligned} A_1 &= \frac{1}{1+M}, & T_1 &= 0, \\ A_2 &= \frac{K}{1+M}, & T_2 &= \frac{T_d}{n}, \\ &\vdots & &\vdots \\ A_i &= \frac{K^{i-1}}{1+M}, & T_i &= \frac{(i-1)\cdot T_d}{n}, \\ &\vdots & &\vdots \\ A_n &= \frac{K^{n-1}}{1+M}, & T_n &= \frac{(n-1)\cdot T_d}{n}, \end{aligned} \tag{5}$$

where $K = \mathrm{e}^{-\left(2\varsigma\pi/\left(n\cdot\sqrt{1-\varsigma^2}\right)\right)}$, $M = K + \cdots + K^{i-1} + K^{n-1}$.

It should be noted that n can be any positive integer larger than 2. The length of the n-impulse shaper is $(n-1)T_d/n$, which increases with the increase of n, and the minimal value is $T_d/2$ if $n = 2$. In this paper, we call any shapers that can realize ZV at the modeling frequency and damping ratio ZV shapers, but we are identifying them by impulse number and a distinguishable character MIS, i.e. 2-, 3-impulse MIS ZV shaper, etc. Here, the character MIS is added to distinguish the shapers obtained by using the MIS technique from those shapers developed by other researchers. The same strategy is also applied to the robust shapers.

If $n = 3$, the 3-impulse MIS ZV shaper becomes

$$\begin{aligned} A_1 &= \frac{1}{1+K+K^2}, \quad T_1 = 0, \\ A_2 &= \frac{K}{1+K+K^2}, \quad T_2 = \frac{T_d}{3}, \\ A_3 &= \frac{K^2}{1+K+K^2}, \quad T_3 = \frac{2T_d}{3}, \end{aligned} \tag{6}$$

where $K = \mathrm{e}^{-\left(2\varsigma\pi/\left(3\sqrt{1-\varsigma^2}\right)\right)}$.

Choosing $\omega = 6.283\,\mathrm{rad/s}$ and $\varsigma = 0.0$, we apply two different shapers in Eqs. (4) and (6) to the vibration system (1). In the simulation, we change the modeling frequency, which is used to design the input shaper, around the natural frequency with a maximal difference of $+/-10\%$ to test the robustness of these two shapers. Figs. 2 and 3 show these simulation results. It can be seen that with the maximal frequency error of $+/-10\%$, the residual vibrations are $+/-17.3$ for the 2-impulse MIS ZV shaper and $+/-12.4\%$ for the 3-impulse MIS ZV shaper, which are too large to be allowed in practice. Thus, input shapers with higher robustness are demanded for practical applications.

Fig. 4 further shows the sensitivity curves of the above two shapers, which demonstrate the relationship between the residual vibration and the frequency ratio. The frequency ratio is the ratio between the natural frequency and the modeling frequency.

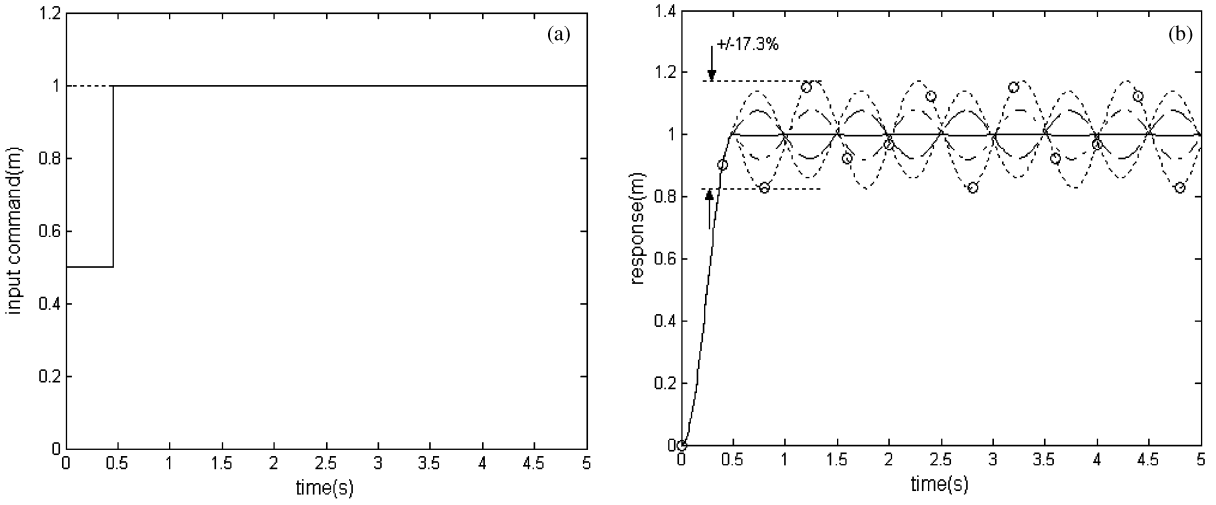

Fig. 2. Simulation result of 2-impulse MIS ZV shaper: (a) input command (dot, unshaped; solid, shaped), (b) response (solid, no error; dash, +5% error; dash–dot, −5% error; dot, +10% error; dot–circle, −10% error).

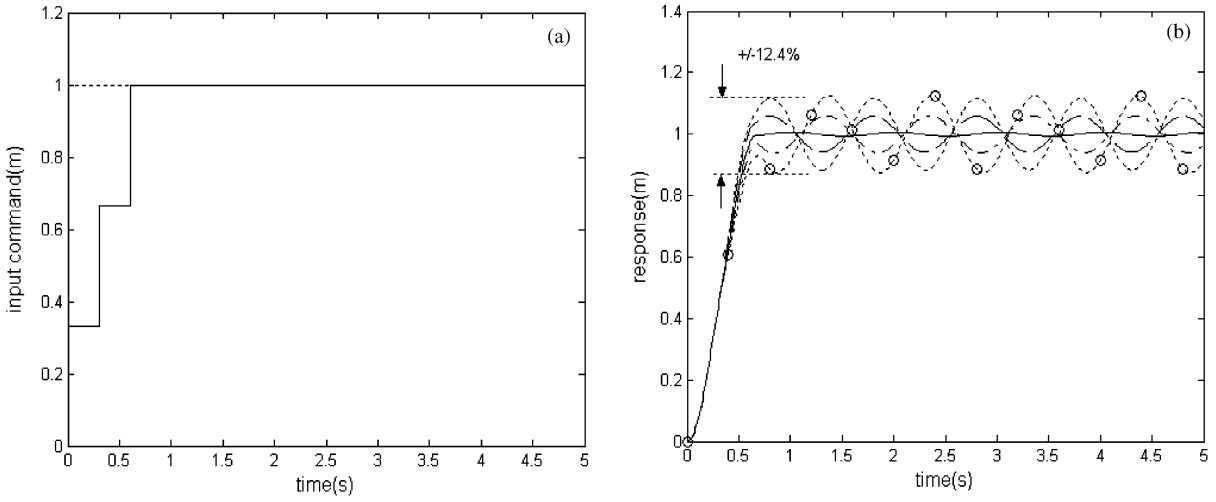

Fig. 3. Simulation result of 3-impulse MIS ZV shaper: (a) input command (dot, unshaped; solid, shaped), (b) response (solid, no error; dash, +5% error; dash–dot, −5% error; dot, +10% error; dot–circle, −10% error).

Given an allowable residual vibration value, we call the frequency ratio range within which the residual vibration is allowable as the insensitivity of the shaper [9]. For example, if 5% residual vibration is allowable, the insensitivities for 2- and 3-impulse MIS ZV shapers are 6.4% (0.968–1.032) and 8.2% (0.96–1.042), respectively.

Moreover, it can be seen from the sensitivity curves in Fig. 4(b) that these two MIS ZV shapers can suppress not only one mode with frequency ratio 1 but also infinite vibration modes with

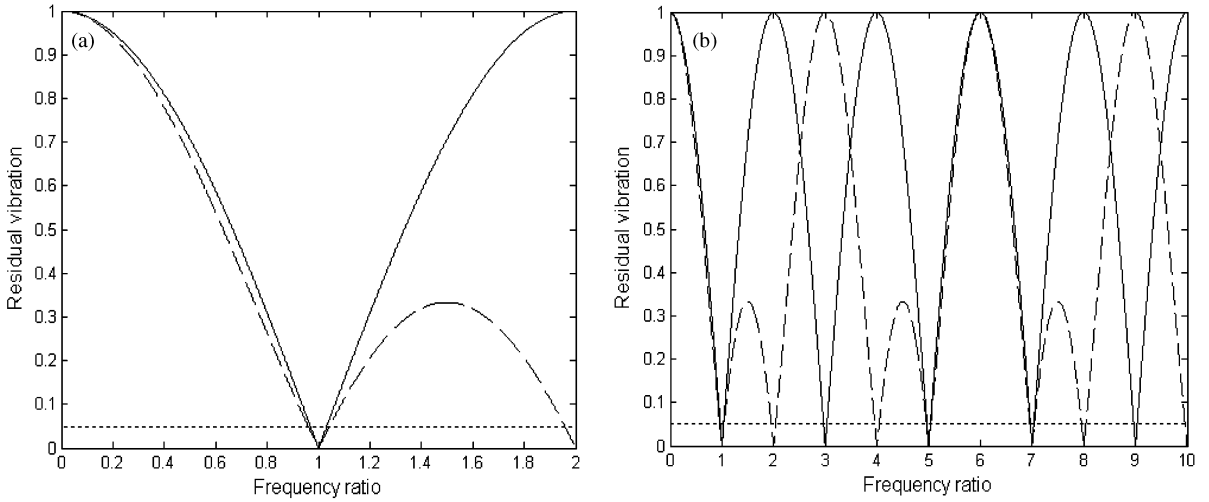

Fig. 4. Sensitivity curves for two MIS ZV shapers: (a) frequency ratio between [0, 2] (solid, 2-impulse MIS ZV; dash, 3-impulse MIS ZV), (b) frequency ratio between [0, 10] (solid, 2-impulse MIS ZV; dash, 3-impulse MIS ZV).

specified frequencies. For the 2-impulse MIS ZV shaper in Eq. (4), it can suppress vibration modes with frequency ratios equal $1, 3, 5, \ldots$, etc. (positive integers except for $2i$). For the 3-impulse MIS ZV shaper in Eq. (6), it can suppress vibration modes with frequency ratios equal $1, 2, 4, 5, \ldots$, etc. (positive integers except for $3i$). In general, we have the following Remark 1 for n-impulse MIS ZV shaper.

Remark 1. If there are n impulses and the amplitudes and acting times satisfy Eq. (5), then the n-impulse MIS shaper can suppress vibration modes with frequency ratios of k, where, k is arbitrary positive integer and $k \neq i \cdot n$.

As discussed previously, robust input shapers are highly demanded for practical application. In TIS technique, the improvement in robustness to system parameter variations can be realized by adding extra constraints [9,34,35]. One such design additionally requires the partial derivatives of the vibration response with respect to frequency and damping to be zero at the modeled frequency and damping. The resultant shaper is known as ZV and derivative (ZVD) shaper, which includes three impulses and has the following expression:

$$A_1 = \frac{1}{1+2K+K^2}, \quad T_1 = 0,$$

$$A_2 = \frac{2K}{1+2K+K^2}, \quad T_2 = \frac{T_d}{2},$$

$$A_3 = \frac{K^2}{1+2K+K^2}, \quad T_3 = T_d, \tag{7}$$

where K is the same as defined in Eq. (4).

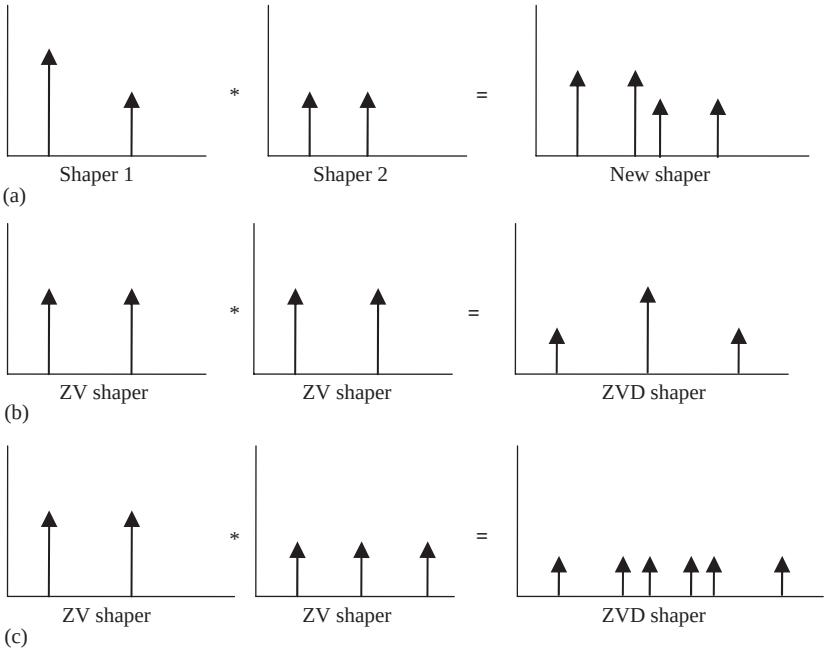

Fig. 5. Convolution process of two shapers: (a) arbitrary two shapers, (b) two identical MIS ZV shapers, (c) two different MIS ZV shapers.

Being different from the TIS, the MIS obtains MIS ZVD shapers by convolving arbitrary two MIS ZV shapers. Fig. 5(a) illustrates the convolving process of two arbitrary 2-impulse shapers. Fig. 5(b) shows the process of convolving two identical 2-impulse MIS ZV shapers that results in the MIS ZVD shaper expressed in Eq. (7). Fig. 5(c) shows another MIS ZVD shaper formed by a 2-impulse MIS ZV shaper and a 3-impulse MIS shaper, which includes 6 impulses and has the following expression:

$$A_1 = \frac{1}{1+M}, \quad T_1 = 0,$$

$$A_2 = \frac{K^2}{1+M}, \quad T_2 = \frac{T_d}{3},$$

$$A_3 = \frac{K^3}{1+M}, \quad T_3 = \frac{T_d}{2},$$

$$A_4 = \frac{K^4}{1+M}, \quad T_4 = \frac{2T_d}{3},$$

$$A_5 = \frac{K^5}{1+M}, \quad T_5 = \frac{5T_d}{6},$$

$$A_6 = \frac{K^7}{1+M}, \quad T_6 = \frac{7T_d}{6}, \tag{8}$$

where $K = e^{-\varsigma\pi/\left(3\sqrt{1-\varsigma^2}\right)}$, $M = K^2 + K^3 + K^4 + K^5 + K^7$.

Eqs. (7) and (8) give the expressions of two MIS ZVD shapers. The same as MIS ZV shapers, there are infinite MIS ZVD shapers according to the MIS technique. We identify MIS ZVD shapers here as $m \times n$-impulse MIS ZVD shapers, where, m and n denote the impulse numbers of two MIS ZV shapers used to form the MIS ZVD shaper. For example, we call the ZVD shapers in Eqs. (7) and (8) 2×2-impulse MIS ZVD shaper and 2×3-impulse MIS ZVD shaper, respectively.

Figs. 6 and 7 show the simulation results when applying these two MIS ZVD shapers to the harmonic vibration system (1). With the maximal $+/-10\%$ error in frequency, now the residual vibrations are only $+/-3\%$ (for the 2×2-impulse MIS ZVD shaper) and $+/-2.21\%$ (for the 2×3-impulse MIS ZVD shaper), respectively. Fig. 8 shows the corresponding sensitivity curves. The insensitivities have been increased to 28.7% (0.8565–1.1435) and 33.18% (0.8429–1.1747), respectively, which are almost 5 times the values of the MIS ZV shapers. The improvement in robustness is remarkable.

It can also be seen from the sensitivity curves in Fig. 8(b) that these two MIS ZVD shapers can suppress vibration and have higher robustness at infinite vibration modes. For the 2×2-impulse MIS ZVD shaper in Eq. (7), it can suppress vibration modes and has higher robustness with frequency ratios equal $1, 3, 5, \ldots$, etc. (positive integers except for $2i$). For the 2×3-impulse MIS ZVD shaper in Eq. (8), it can suppress vibration modes when frequency ratios equal $1, 2, 3, 4, 5, 7, \ldots$ (positive integers except for $6i$), and has higher robustness when frequency ratios equal $1, 5, 7, 11, 13, \ldots$, etc. (positive integers except for $2i$ and $3i$).

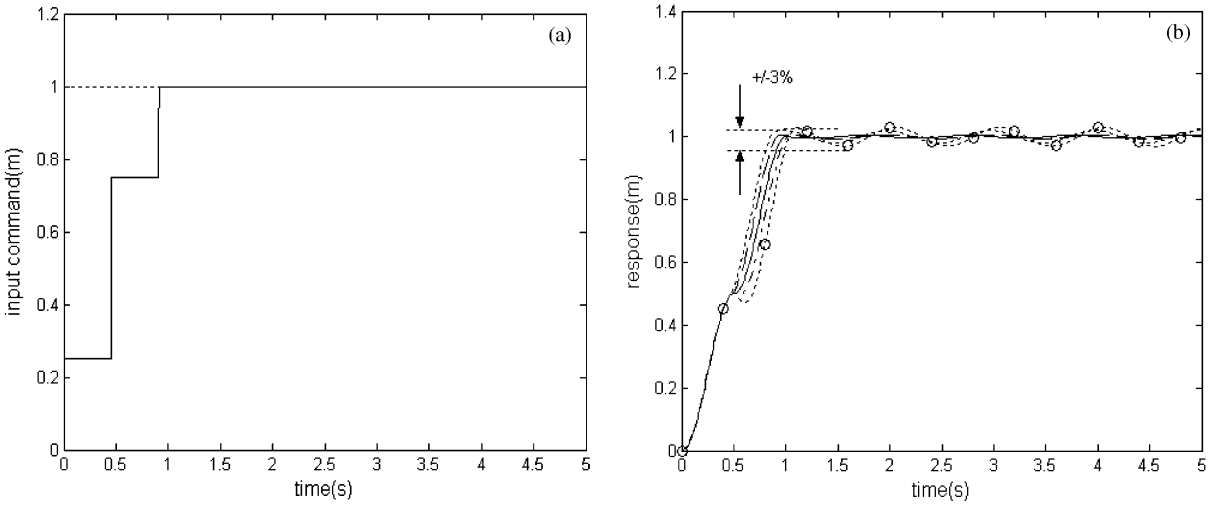

Fig. 6. Simulation result of 2×2-impulse MIS ZVD shaper: (a) input command (dot, unshaped; solid, shaped), (b) response (solid, no error; dash, +5% error; dash–dot, −5% error; dot, +10% error; dot–circle, −10% error).

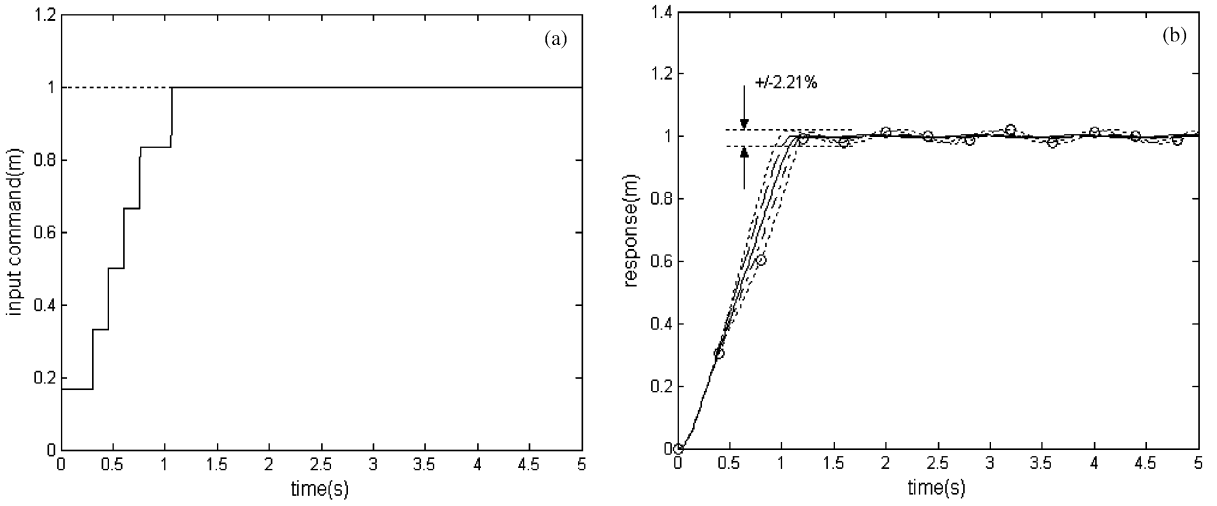

Fig. 7. Simulation result of 2×3-impulse MIS ZVD shaper: (a) input command (dot, unshaped; solid, shaped), (b) response (solid, no error; dash, +5% error; dash–dot, −5% error; dot, +10% error; dot–circle, −10% error).

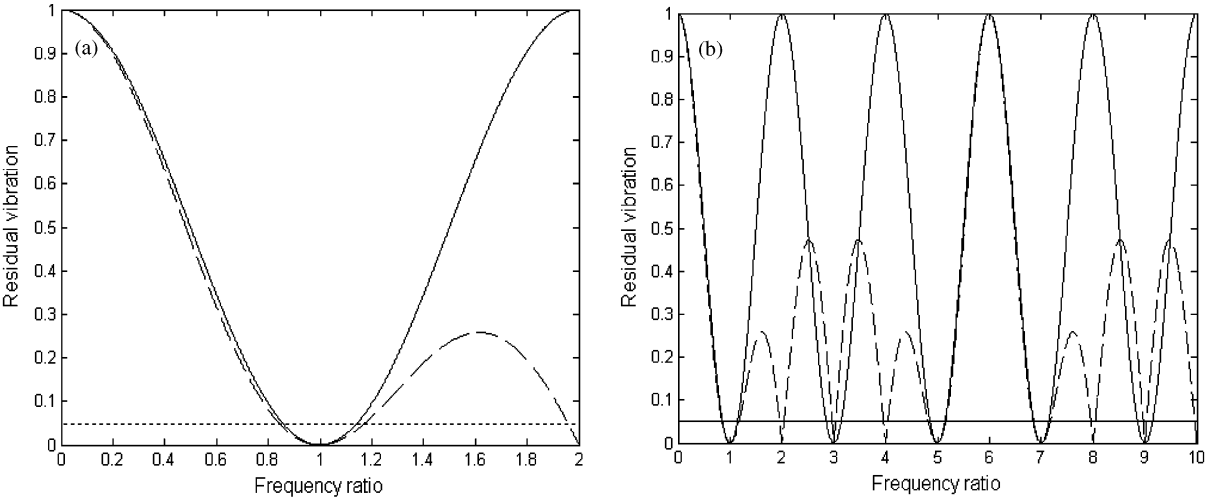

Fig. 8. Sensitivity curve for two MIS ZVD shapers: (a) frequency ratio between $[0, 2]$ (solid, 2×2-impulse MIS ZVD; dash, 2×3-impulse MIS ZVD), (b) frequency ratio between $[0, 10]$ (solid, 2×2-impulse MIS ZVD; dash, 2×3-impulse MIS ZVD).

Remark 2. The $m \times n$-impulse MIS ZVD shaper can suppress vibration modes when frequency ratios equal f_{ZV} ($f_{ZV} \neq i \cdot$ LCM, where LCM is the least common multiple of m and n). Moreover, it will have higher robustness for vibration modes with frequency ratios equal to f_{ZVD}, where $f_{ZVD} \neq i \cdot m$ and $f_{ZVD} \neq i \cdot n$.

The sensitivity curves for the four shapers, i.e. 2-impulse MIS ZV, 3-impulse MIS ZV, 2×2-impulse MIS ZVD, and 2×3-impulse MIS ZVD, are given in Fig. 9 for further comparison.

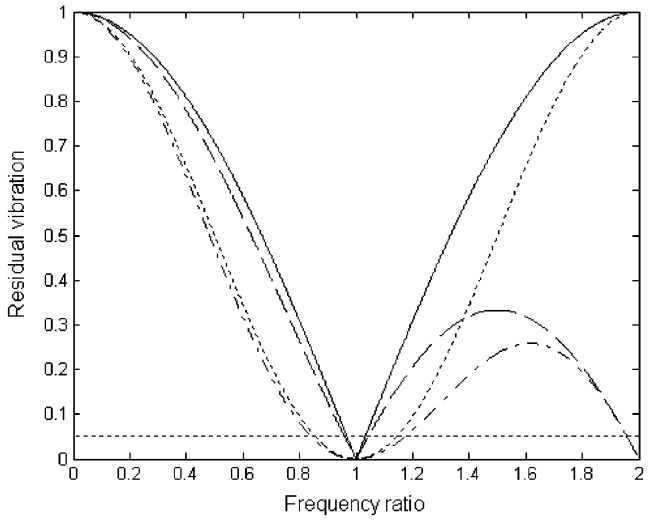

Fig. 9. Sensitivity curve for four shapers (solid, 2-impulse MIS ZV; dash, 3-impulse MIS ZV; dot, 2 × 2-impulse MIS ZVD; dash–dot, 2 × 3-impulse MIS ZVD).

Sharing the same principle, (1) the shapers with higher robustness can be obtained by convolving multiple shapers with lower robustness; and (2) an arbitrary number of shapers can be convolved to form a new shaper with expected robustness and characteristics. For example, the convolution of a 2-impulse MIS ZV shaper with a 2 × 3-impulse MIS ZVD shaper can result in a 2 × 2 × 3-impulse MIS ZVDD shaper; the convolution of a 2 × 2-impulse MIS ZVD shaper with a 2 × 3-impulse MIS ZVD shaper can result in a more robust 2 × 2 × 2 × 3-impulse MIS ZVDDD shaper, etc.

Remark 3. The previous analysis and simulation show that the shapers with arbitrary robustness and/or with the ability of multimode suppression can be formed by using the proposed MIS technique. However, the designer should be aware that the improvements in performance are at the cost of increases in length of shapers. For example, the lengths for the 2-impulse MIS ZV shaper in Eq. (4), 3-impulse MIS ZV shaper in Eq. (6), 2 × 2-impulse MIS ZVD shaper in Eq. (7) and 2 × 3-impulse MIS ZVD shaper in Eq. (8) are $T_d/2$, $2T_d/3$, T_d and $7T_d/6$. The better the ability of vibration suppression is, the longer the shaper will be.

3. Dynamic modeling

A single-link flexible manipulator grasping a payload is modeled as a uniform cantilever beam with a tip mass that can rotate about the Z-axis perpendicular to the paper, as shown in Fig. 10. For system modeling, the following assumptions are made: (1) the beam is considered to be an Euler–Bernoulli beam and the axial deformation is neglected; (2) the gravitational effect and the hub dynamics are neglected for simplicity.

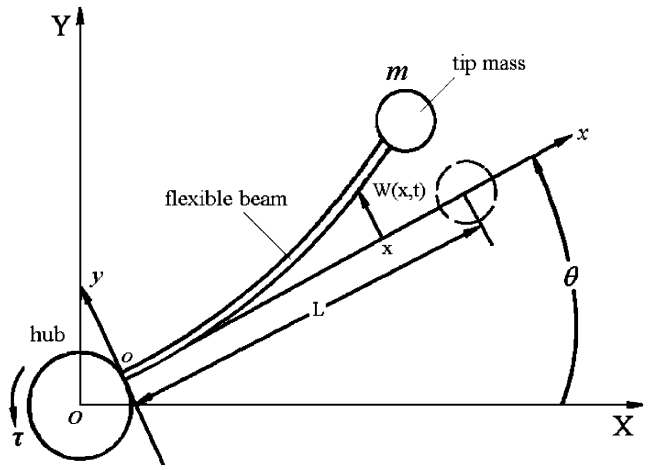

Fig. 10. A single-link flexible manipulator.

Applying Lagrange's approach, the motion of the complete system equation is represented by

$$\underbrace{\begin{bmatrix} m_{\theta\theta} & m_{\theta q} \\ m_{\theta q}^T & m_{qq} \end{bmatrix}}_{M(q)} \begin{bmatrix} \ddot{\theta} \\ \ddot{q} \end{bmatrix} + \underbrace{\begin{bmatrix} \dot{q}^{\mathrm{T}} m_{qq} q & \dot{\theta} q^{\mathrm{T}} m_{qq} \\ -\dot{\theta} m_{qq} q & 0 \end{bmatrix}}_{C(\dot{\theta},q,\dot{q})} \begin{bmatrix} \dot{\theta} \\ \dot{q} \end{bmatrix} + \begin{bmatrix} 0 \\ K_q q \end{bmatrix} = \begin{bmatrix} \tau \\ 0 \end{bmatrix}, \tag{9}$$

where θ represents the hub angle, q is the flexible deflection, $m_{\theta\theta}$, m_{qq}, $m_{\theta q}$ are parameters related to the inertia, K_q is the stiffness matrix, τ denotes the input torque acting on the hub. Moreover, $\frac{1}{2}\dot{M}(q) - C(\dot{\theta}, q, \dot{q})$ is a skew symmetric matrix.

4. Experiments

Fig. 11 shows a photograph of the experimental single-link flexible manipulator developed to verify the approach proposed in this paper. This setup consists of a flexible aluminum beam and a SANYO servo AC motor with a gear reduction of 1:25. The light-weight flexible beam is clamped at the shaft of the motor through a coupling and is limited to rotate only in the horizontal plane, so the effect of gravity can be ignored. The tip deflection of the link is measured by a system consisting of a laser diode, which locates at the hub, and a position-sensitive detector (PSD), which is installed at the tip of the flexible link. The measurement range of the PSD is ± 8 mm. A built-in incremental encoder is used to calculate the rotating angle of the hub. The encoder has the resolution of 0.0072° per pulse. A three-axis quadrature encoder and counter card, PCL-833, is used to count the encoder pulses. The analogue signal of the PSD is converted into digital data through a PCL-818HD A/D card. The control voltage for driving the motor is sent to the servo amplifier through a PCL-727 D/A card. Moreover, different mode characteristics can be obtained by bonding the PZT layer at different positions.

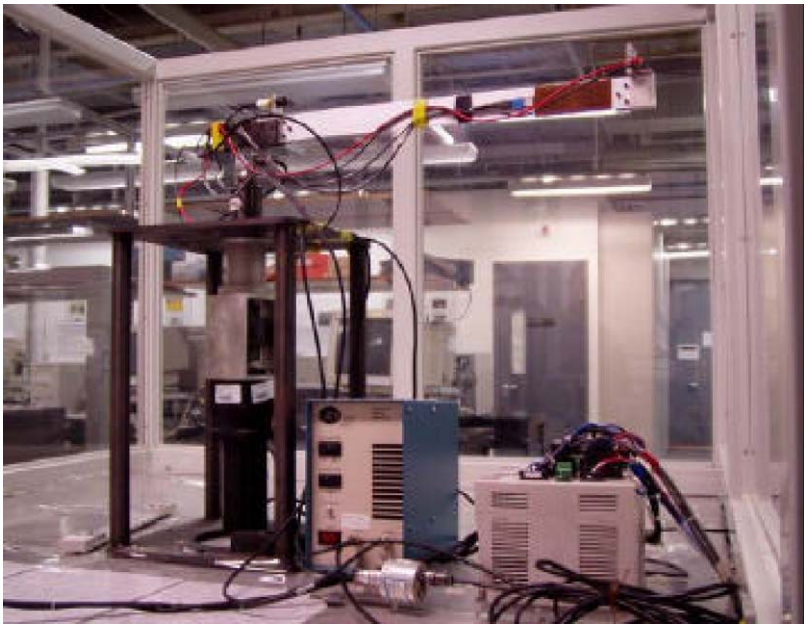

Fig. 11. Photographs of the experimental single-link flexible manipulator.

To identify the mode characteristic of the flexible system, we apply bang–bang commands to drive the motor and implement the fast Fourier transform (FFT) to the measured tip deflection. Fig. 12 shows the measured tip deflection curve and the corresponding result of FFT. Here, a third-order bandpass Butterworth digital filter with passband frequency of 0.5–20 Hz (3.14–125.6 rad/s) is applied to pre-filter the measured data in order to reduce the low-frequency offset and the high-frequency noise. It can be seen that the first two modes play the main roles in the vibration. The frequencies of these two modes are 25.1529 and 50.2655 rad/s, respectively. For the damping ratio, we calculated it on the basis of decay characteristic of the measured vibration signal. The mode parameters of the experimental flexible manipulator are listed in Table 1.

4.1. Controller design

In this section, we first propose a PD feedback control law for the hub angle motion of the single-link flexible manipulator. Second, various input shapers are designed according to the measured frequencies and damping ratios to shape the angle commands. Finally, the shaped commands are sent to the controller as the final input commands. Using this strategy, the vibration modes are expected to be suppressed effectively while achieving the desired attitude motion. It should be noted that the frequencies and damping ratios of the flexible manipulator with PD feedback controller will be different from those values obtained by applying the open-loop bang–bang commands. These differences are small for our flexible system because it has a large gear reduction and a light flexible beam. However, for the convenience of robustness analysis, it is a good choice to use the measured frequencies and damping ratios in Table 1 (with errors) for designing of the MIS.

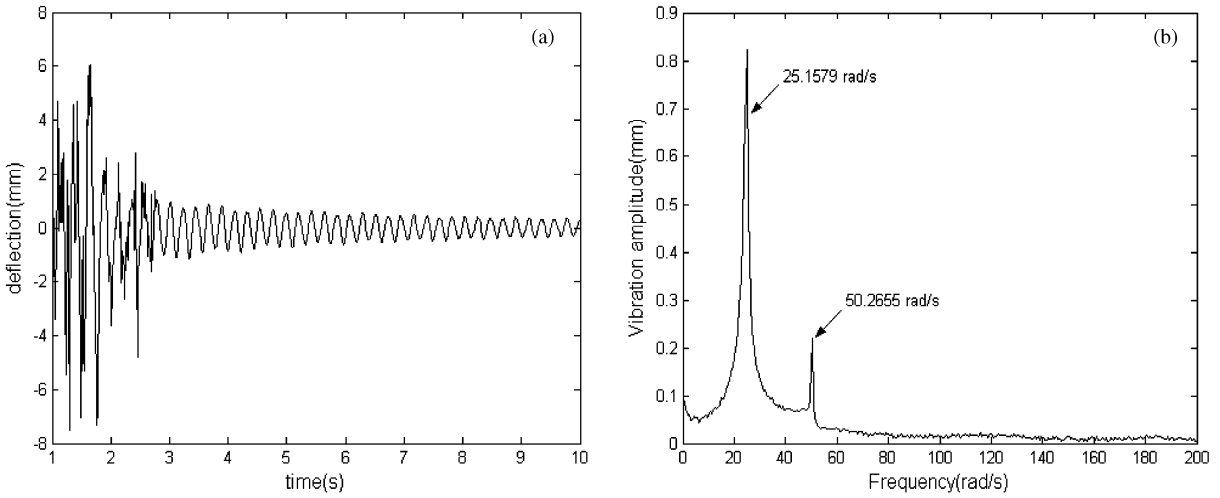

Fig. 12. Mode identification of the experimental flexible manipulator: (a) tip deflection curve, (b) FFT result.

Table 1
Mode parameters of the experimental flexible manipulator

Parameter	The first mode	The second mode	Unit
Frequency	25.1529	50.2655	rad/s
Damping ratio	0.0045	0.004	

4.1.1. PD controller for rigid motion

The following PD feedback controller was designed to drive the motor:

$$\tau(t) = -K_P e(t) - K_D \dot{e}(t), \tag{10}$$

where $e(t) = \theta(t) - \theta_d$ and $\dot{e}(t) = \dot{\theta}(t) - \dot{\theta}_d$ are angle position error and angular velocity error, respectively; K_P and K_D are proportional and derivative gains.

To compensate for the motor friction, the practical control torque, τ_p, was defined by

$$\tau_p(t) = \tau(t) + 0.002\dot{\theta}(t) + 0.005\,\mathrm{sgn}(\dot{\theta}(t)), \tag{11}$$

where $\tau(t)$ is the same as in Eq. (10), and the remaining two terms denote the feedforward compensations of the viscous and Coulomb frictions. The compensation coefficients are selected experimentally.

4.1.2. MIS for vibration suppression

In this section, we will design various input shapers using the MIS technique, based on the measured frequencies and damping ratios. Considering the mode condition of the flexible manipulator, we select the first two vibration modes as the targeted modes to suppress.

From the modes' parameters listed in Table 1, we know that the frequency of the second mode almost equals twice the frequency of the first mode, i.e., $25.1529 \times 2 = 50.3058 \cong 50.2655\,\text{rad/s}$. According to Remarks 1 and 2 in Section 2, if a 3-impulse MIS ZV shaper designed for suppressing the first mode is applied, this shaper can also suppress the second mode; if a 2×3-impulse MIS ZVD shaper is designed to suppress the first vibration mode, it can suppress these two modes and will enhance the robustness for suppressing the first mode. However, in TIS, we have to convolve two ZV shapers, each for one mode, to get the 4-impulse TIS ZV shaper that can suppress two modes. To get a shaper that has the ability of a 2×3-impulse MIS ZVD shaper, three ZV shapers must be convolved together, two ZV shapers for the first mode and the other for the second mode. Thus, to get an appropriate shaper, the MIS is much simpler than the traditional technique.

In the following, four MIS shapers, 2-impulse MIS ZV, 3-impulse MIS ZV, 2×2-impulse MIS ZVD, and 2×3-impulse MIS ZVD shapers, are designed according to the mode parameters in Table 1 and then these shapers will be applied in the hardware experiments to verify the MIS technique:

2-*impulse MIS ZV shaper*:

$$\begin{bmatrix} A_i \\ t_i \end{bmatrix} = \begin{bmatrix} 0.5035 & 0.4965 \\ 0 & 0.1249 \end{bmatrix}. \tag{12}$$

3-*impulse MIS ZV shaper*:

$$\begin{bmatrix} A_i \\ t_i \end{bmatrix} = \begin{bmatrix} 0.3365 & 0.3333 & 0.3302 \\ 0 & 0.0833 & 0.1665 \end{bmatrix}. \tag{13}$$

2×2-*impulse MIS ZVD shaper*:

$$\begin{bmatrix} A_i \\ t_i \end{bmatrix} = \begin{bmatrix} 0.2535 & 0.5000 & 0.2465 \\ 0 & 0.1249 & 0.2498 \end{bmatrix}. \tag{14}$$

2×3-*impulse MIS ZVD shaper*:

$$\begin{bmatrix} A_i \\ t_i \end{bmatrix} = \begin{bmatrix} 0.1694 & 0.1678 & 0.1671 & 0.1663 & 0.1655 & 0.1639 \\ 0 & 0.0833 & 0.1249 & 0.1665 & 0.2082 & 0.2914 \end{bmatrix}. \tag{15}$$

4.2. Experimental results

Experiments are conducted on the system shown in Fig. 11. The goal is to rotate the hub position to a desired angle 30° while suppressing flexible vibration effectively. In the following experiments, the unshaped reference input of the motor is a 30° step command. The feedback coefficients of the PD controller (10) are chosen experimentally to realize a good-compromise hub-angle response in terms of overshoot, rising time and settling time, and no PSD measuring over-range. The sampling frequency is set to 1 ms and the final gains are chosen as

$$K_P = 0.05, \quad K_D = 0.01. \tag{16}$$

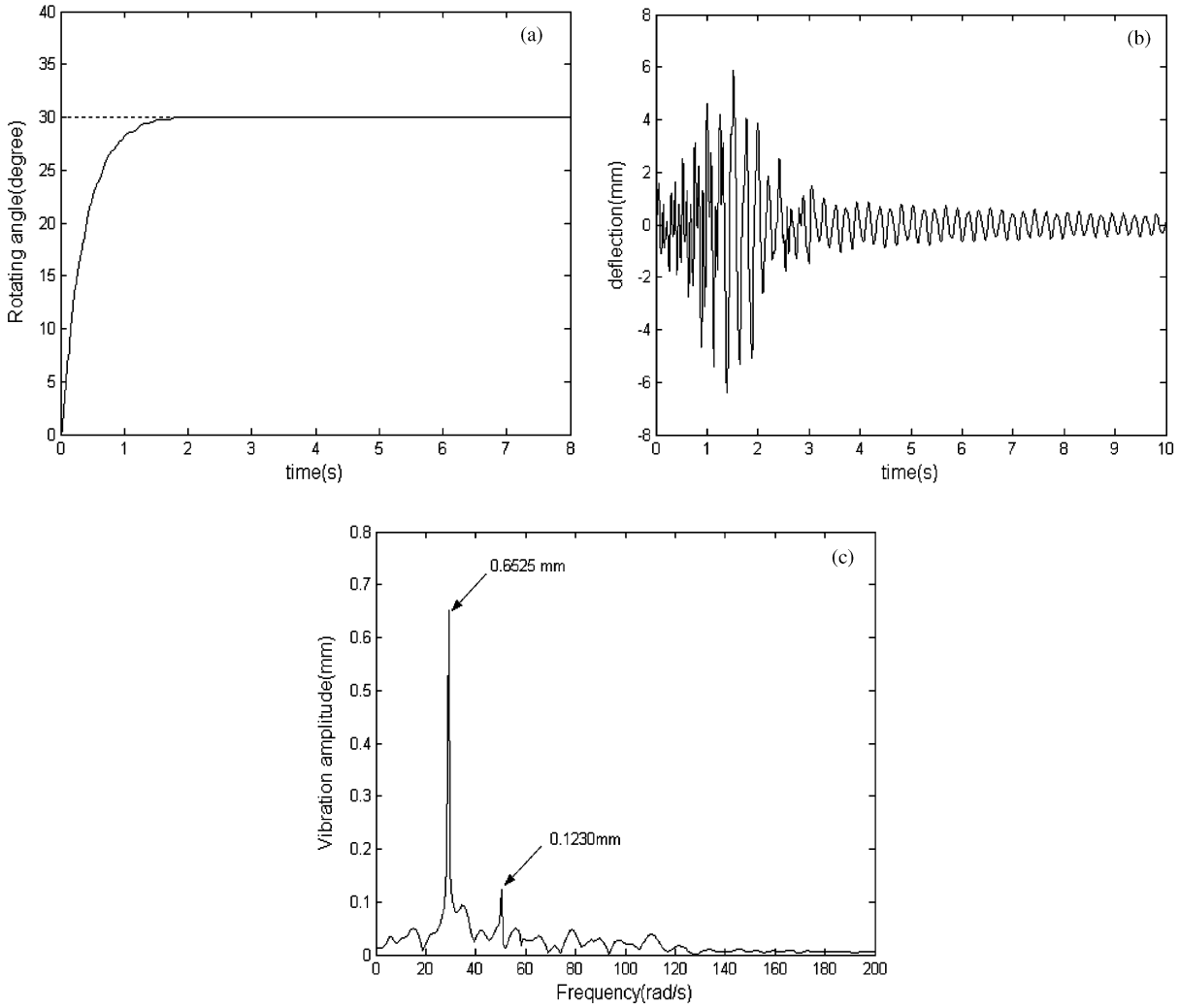

Fig. 13. Experimental results of maneuvering without shaping: (a) attitude angle motion (dot, desired angle; dash, actual angle), (b) tip deflection curve, (c) FFT of PSD measurement.

For comparison, the experiment of using PD feedback only is carried out first and the result is shown in Fig. 13. Then, experiments of combining the PD controller with four different MIS in Eqs. (12), (13), (14), and (15) are conducted, and the results are shown in Figs. 14–17. The FFT amplitudes of residual vibration without/with MIS are listed in Table 2.

From the experimental results we know that, with the PD controller without input shaping, the amplitudes of the first two vibration modes are 0.6525 and 0.123 mm, respectively, after slewing. Comparing this result, the tip deflection has been effectively suppressed by combining MIS with the PD controller; see Figs. 14–17. With the 2-impulse MIS ZV shaper in Eq. (12), these two amplitudes are 0.1093 and 0.0914 mm as this MIS shaper has the ability of suppressing the first vibration mode only. With the 3-impulse MIS ZV shaper in Eq. (13), both amplitudes

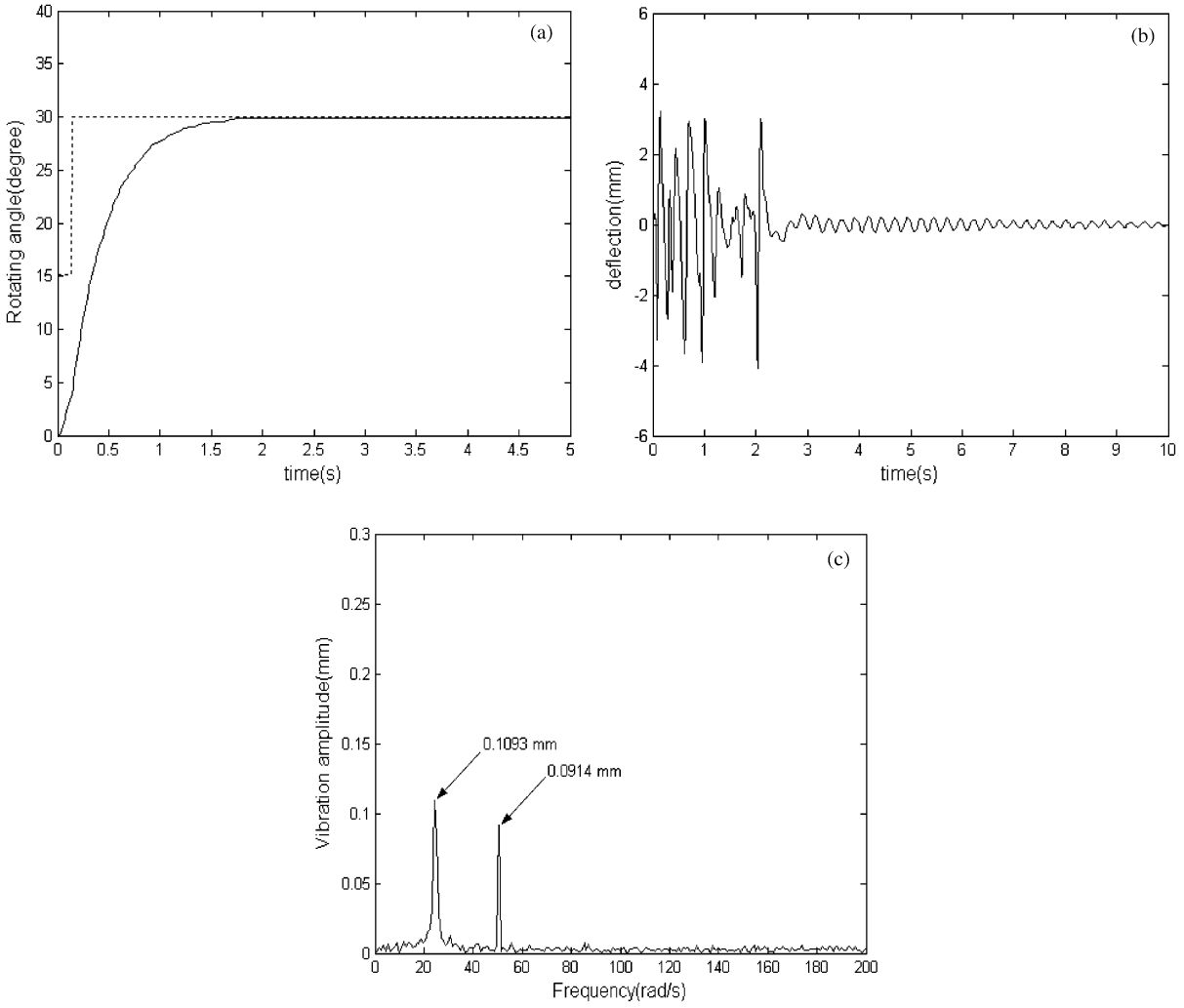

Fig. 14. Experimental results of maneuvering with 2-impulse MIS ZV shaper: (a) attitude angle motion (dot, desired angle; dash, actual angle), (b) tip deflection curve, (c) FFT of PSD measurement.

are reduced to 0.0969 and 0.0351 mm because this MIS shaper can suppress these two modes together. The amplitudes of the first mode are suppressed to be 0.0505 and 0.0313 mm when using the robust 2×2-impulse and 2×3-impulse MIS ZVD shapers in Eqs. (14) and (15). Moreover, for the second vibration mode, we obtained the smallest amplitude, 0.011 mm, using the 2×3-impulse MIS ZVD shaper because this shaper has the ability of suppressing the second vibration mode. However, with the 2×2-impulse MIS ZVD shaper, the amplitude of the second mode is 0.0903 mm, which is almost the same as the value obtained by the 2-impulse MIS ZV shaper. These results are reasonable because they cannot suppress the second vibration mode.

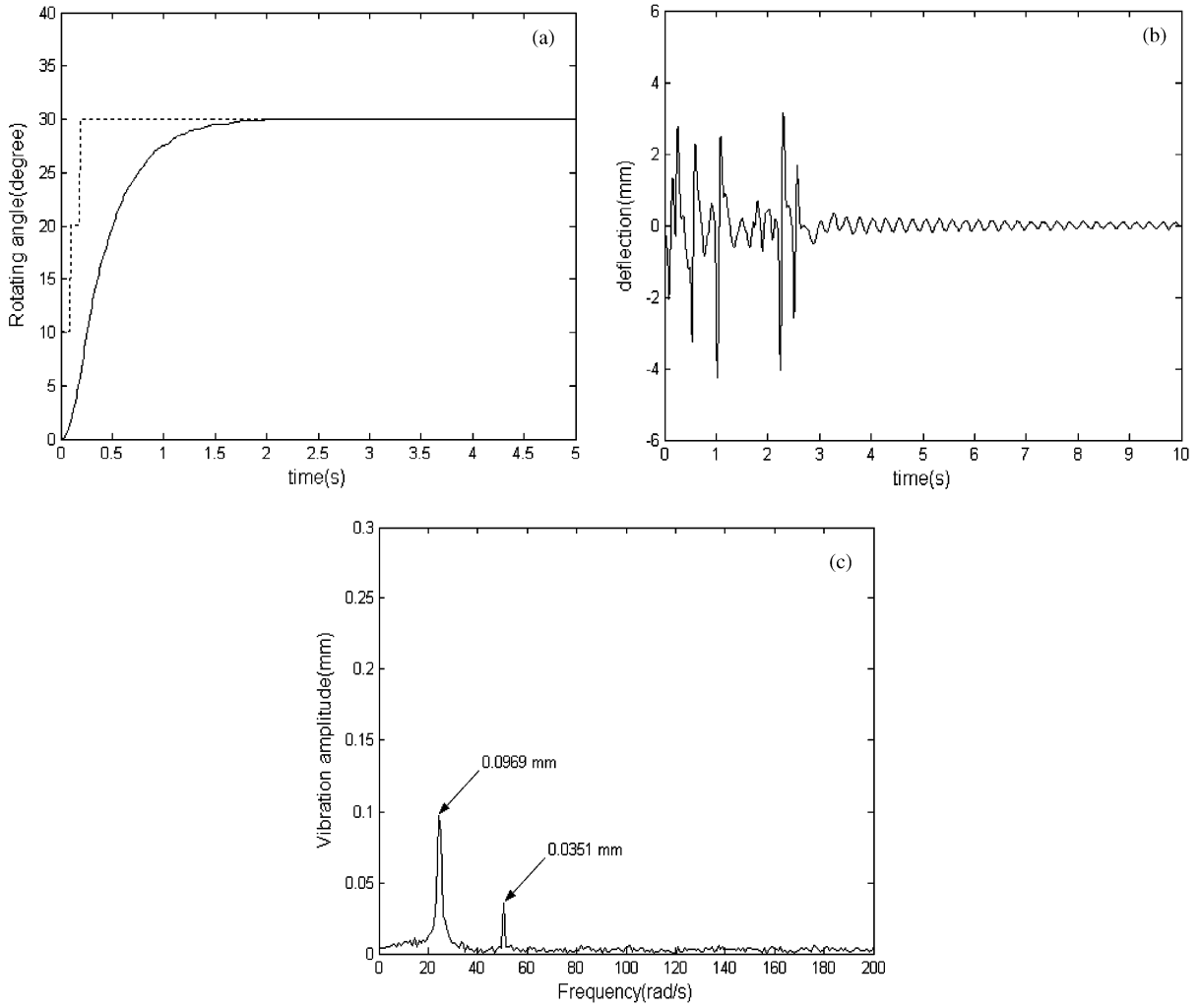

Fig. 15. Experimental results of maneuvering with 3-impulse MIS ZV shaper: (a) attitude angle motion (dot, desired angle; dash, actual angle), (b) tip deflection curve, (c) FFT of PSD measurement.

For making a complete comparison between various input shapers, we also calculate the lengths of these shapers and list the values in Table 2. We also consider two TIS: TIS two-mode ZV (one ZV shaper for each vibration mode) and TIS two-mode ZVD-ZV (ZVD shaper for the first mode and ZV shaper for the second modes). The results show that the 2-impulse MIS shaper has the shortest length, 0.1249 s. However, it can only suppress the first vibration mode and has no robustness. For two shapers that all can suppress the first two vibration modes concurrently, 3-impulse MIS ZV has a length of 0.1665 s. However, the TIS two-mode ZV has a longer length, 0.1874 s. Similarly, the 2×3-impulse MIS ZVD has a shorter length, 0.2914 s, than the TIS two-mode ZVD-ZV, 0.3123 s.

Furthermore, we have conducted experiments on different system configurations and obtained satisfactory results. However, those results are not shown in this paper.

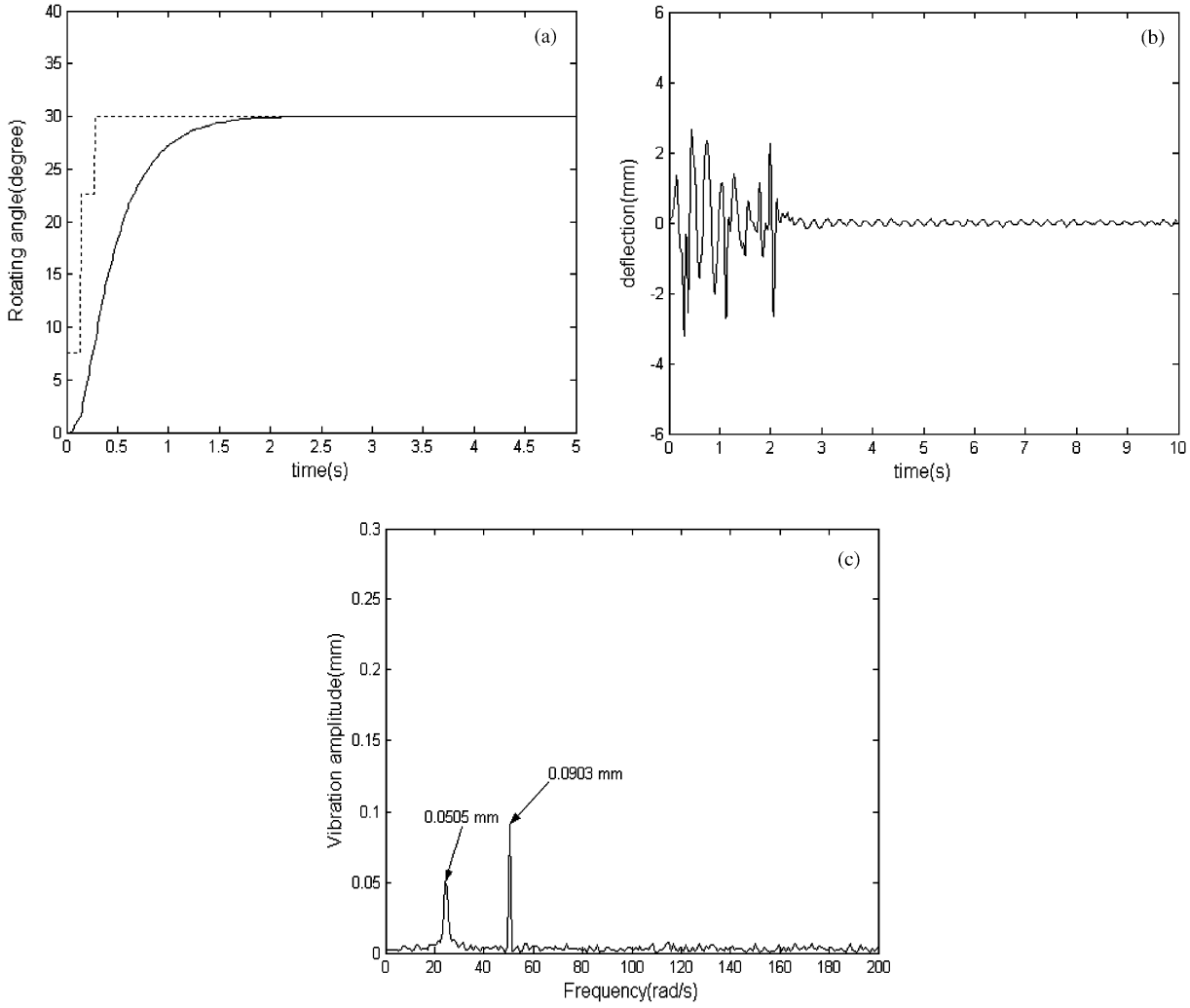

Fig. 16. Experimental results of maneuvering with 2×2-impulse MIS ZVD shaper: (a) attitude angle motion (dot, desired angle; dash, actual angle), (b) tip deflection curve, (c) FFT of PSD measurement.

5. Conclusions

Input shaping is an effective vibration control method that has been widely studied in recent years. In this paper, the modified input shaping (MIS) method is proposed to get better performance. The MIS method is analyzed in detail and has been compared with the traditional input shaping (TIS) method. First, it is shown that the length of a MIS shaper is shorter than that of a corresponding TIS shaper while both shapers have the same ability of vibration suppression. Second, the MIS method is easier than the traditional method because the numerical optimization is unnecessary in the design of the MIS shaper. However, to get a satisfactory shaper with the TIS method, optimization is necessary. For a single-link flexible manipulator, the MIS method is

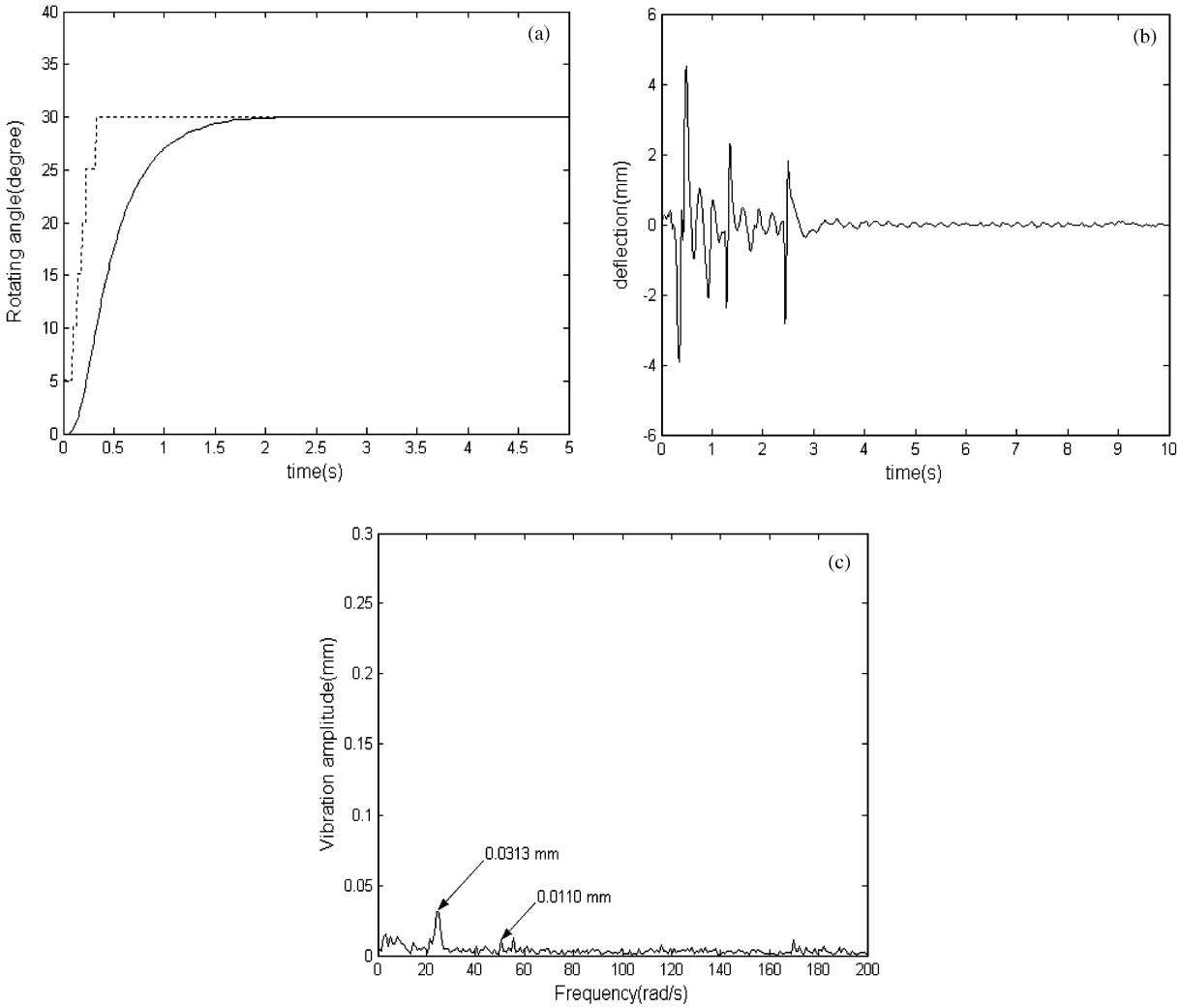

Fig. 17. Experimental results of maneuvering with 2 × 3-impulse MIS ZVD shaper: (a) attitude angle motion (dot, desired angle; dash, actual angle), (b) tip deflection curve, (c) FFT of PSD measurement.

Table 2
Comparison between various input shapers: MIS and TIS

Type of shaper	1st mode (mm)	2nd mode (mm)	Length (s)	Performance
N/A	0.6525	0.1230	0	N/A
2-impulse MIS ZV	0.1093	0.0914	0.1249	1st mode
3-impulse MIS ZV	0.0969	0.0351	0.1665	1st, 2nd mode
2 × 2-impulse MIS ZVD	0.0505	0.0903	0.2498	1st mode, robust
2 × 3-impulse MIS ZVD	0.0313	0.0110	0.2914	1st mode, robust; 2nd mode
TIS two-mode ZV			0.1874	1st, 2nd mode
TIS two-mode ZVD-ZV			0.3123	1st mode, robust; 2nd mode

combined with a PD feedback controller to suppress flexible vibration while realizing the hub motion. Several MIS shapers, non-robust and robust, are designed for the flexible manipulator. Experimental results validate the proposed approach and the theoretical analysis.

Acknowledgements

The authors would like to thank the anonymous reviewers for their valuable comments and suggestions, which significantly improved the quality of this paper.

References

[1] W.J. Book, Controlled motion in an elastic world, *ASME Journal of Dynamic Systems, Mesurement, and Control* 115 (1) (1993) 252–261.
[2] D.C. Hyland, J.L. Junkins, R.W. Longman, Active control technology for large space structures, *Journal of Guidance, Control, and Dynamics* 16 (5) (1993) 801–821.
[3] H.B. Brown, V. Feliu, K.S. Rattan, Adaptive control of a single-link flexible manipulator, *IEEE Control Systems Magazine* 10 (2) (1990) 29–33.
[4] W.A. Kwong, V.G. Moudgal, K.M. Passino, S. Yurkovich, Fuzzy learning control for a flexible-link robot, *IEEE Transactions on Fuzzy Systems* 3 (2) (1995) 199–210.
[5] S.B. Choi, C.C. Cheong, H.C. Shin, Sliding mode control of vibration in a single-link flexible arm with parameter variations, *Journal of Sound and Vibration* 179 (1995) 737–748.
[6] M.K. Sundareshan, C. Askew, Neural network-assisted variable structure control scheme for control of a flexible manipulator arm, *Automatica* 33 (9) (1997) 1699–1710.
[7] H.C. Shin, S.B. Choi, Position control of a two-link flexible manipulator featuring piezoelectric actuators and sensors, *Mechatronics* 11 (6) (2001) 707–729.
[8] C. Liang, C.A. Rogers, Design of shape memory alloy springs with applications in vibration control, *ASME Transaction Journal of Vibration and Acoustics* 115 (1) (1993) 129–135.
[9] N.C. Singer, W.P. Seering, Preshaping command inputs to reduce system vibration, *Journal of Dynamics Systems, Measurement and Control* 112 (1) (1990) 76–82.
[10] S.D. Jones, A.G. Ulsoy, Control input shaping for coordinate measuring machines, *Proceedings of the American Control Conference*, Baltimore, MD, June–July 1994.
[11] W.E. Singhose, N.C. Singer, W.P. Seering, Improving repeatability of coordinate measuring machines with shaped command signals, *Precision Engineering* 18 (2–3) (1996) 138–146.
[12] T.D. Tuttle, W.P. Seering, Vibration reduction in 0-g using input shaping on the MIT middeck active control experiment, *Proceedings of the American Control Conference*, Seattle, WA, June 1995.
[13] T.D. Tuttle, W.P. Seering, Vibration reduction in flexible space structures using input shaping on MACE: mission results, *Proceedings of the IFAC World Congress*, San Francisco, CA, June 1996.
[14] J.F. Jansen, Control and analysis of a single-link flexible beam with experimental verification, ORNL/TM-12198, Oak Ridge National Laboratory, 1992.
[15] N.C. Singer, W.E. Singhose, E. Kriikku, An input shaping controller enabling cranes to move without sway, *Proceedings of the ANS Seventh Topical Meeting on Robotics and Remote Systems*, Augusta, GA, April–May 1997.
[16] M. Kennison, W.E. Singhose, Input shaper design for double-pendulum planar gantry cranes, *Proceedings of the IEEE Conference on Control Applications*, Hawaii, August 1999.
[17] W.E. Singhose, N.C. Singer, Effects of input shaping on two-dimensional trajectory following, *IEEE Transactions on Robotics and Automation* 12 (6) (1996) 881–887.
[18] K.L. Hillsley, S. Yurkovich, Vibration control of a two-link flexible robot arm, *Journal of Dynamics and Control Systems* 3 (2) (1993) 261–280.

[19] V. Drapeau, D. Wang, Verification of a closed-loop shaped-input controller for a five-bar-linkage manipulator, *Proceedings of the IEEE Conference on Robotics and Automation*, Atlanta, GA, May 1993.
[20] D.P. Magee, W.J. Book, Filtering micro-manipulator wrist commands to prevent flexible base motion, *Proceedings of the American Control Conference*, Seattle, WA, June 1995.
[21] E.A. Ooten, W. Singhose, Command generation with sliding mode control for flexible systems, *Proceedings of the International Symposium on Motion and Vibration Control in Mechatronics*, Tokyo, Japan, 1999.
[22] B.R. Murphy, I. Watanabe, Digital shaping filters for reducing machine vibration, *IEEE Transactions on Robotics and Automation* 8 (2) (1992) 285–289.
[23] T. Singh, S.R. Vadali, Robust time-delay control, *ASME Journal of Dynamic Systems, Measurement, and Control* 115 (2) (1993) 303–306.
[24] T.D. Tuttle, W.P. Seering, A zero-placement technique for designing shaped inputs to suppress multiple-mode vibration, *Proceedings of the American Control Conference*, Baltimore, MD, June–July 1994.
[25] U.-H. Park, J.-W. Lee, B.-D. Lim, Y.-G. Sung, Design and sensitivity analysis of an input shaping filter in Z-plane, *Journal of Sound and Vibration* 243 (2001) 157–171.
[26] L.Y. Pao, Multi-input shaping design for vibration reduction, *Automatica* 35 (1) (1999) 81–89.
[27] Q. Liu, B. Wei, Robust time-optimal control of uncertain flexible spacecraft, *Journal of Guidance, Control, and Dynamics* 15 (3) (1992) 597–604.
[28] W.E. Singhose, N.C. Singer, W.P. Seering, Time-optimal negative input shapers, *Journal of Dynamic Systems, Measurement, and Control* 119 (2) (1997) 198–205.
[29] N.C. Singer, W.E. Singhose, W.P. Seering, Comparison of filtering methods for reducing residual vibration, *European Journal of Control* 5 (2) (1999) 208–218.
[30] J.M. Hyde, W.P. Seering, Using input command pre-shaping to suppress multiple mode vibration, *Proceedings of the IEEE Conference on Robotics and Automation*, Sacramento, CA, April 1991.
[31] W.E. Singhose, E.A. Crain, W.P. Seering, Convolved and simultaneous two-mode input shapers, *IEE Proceedings Control Theory and Applications* 144 (6) (1997) 515–520.
[32] O.J.M. Smith, *Feedback Control System*, McGraw-Hill Book Company, Inc., New York, 1958.
[33] J. Shan, D. Sun, D. Liu, Design for robust component synthesis vibration suppression of flexible spacecrafts with on–off actuators, *IEEE Transactions on Robotics and Automation* 20 (3) (2004) 512–525.
[34] W.E. Singhose, L. Porter, N.C. Singer, Vibration reduction using multi-hump extra-insensitive input shapers, *Proceedings of the American Control Conference*, Seattle, WA, June 1995.
[35] W.E. Singhose, S. Derezinski, N.C. Singer, Extra-insensitive input shapers for controlling flexible spacecraft, *Journal of Guidance, Control, and Dynamics* 19 (2) (1996) 385–391.